Journal of Solid State Chemistry 182 (2009) 147–152

Contents lists available at ScienceDirect

Journal of Solid State Chemistry

journal homepage: www.elsevier.com/locate/jssc

Unusual spin gap transition observed in two new molecular magnets based on $[Ni(mnt)_2]^-$ monoanion (mnt^{2-} = maleonitriledithiolate)

Hong-rong Zuo [a], Qian Huang [a], Chun-yan Huang [a], Dong-hai Huang [a], Yong Hou [a], Le-min Yang [a], Chun-lin Ni [a,*], Qing-jin Meng [b]

[a] Department of Applied Chemistry, Centre of Inorganic Functional Materials, College of Science, South China Agricultural University, 510642 Guangzhou, PR China
[b] State Key Laboratory of Coordination Chemistry, Coordination Chemistry Institute, Nanjing University, 210093 Nanjing, PR China

ARTICLE INFO

Article history:
Received 1 July 2008
Received in revised form
7 October 2008
Accepted 13 October 2008
Available online 22 October 2008

Keywords:
Bis(maleonitriledithiolato)nickelate monoanion
Molecular magnet
Substituted benzyl-4-dimetylaminopyridinium
Crystal structures
Spin gap transition

ABSTRACT

Two new molecular magnets, $[RBzPyN(CH_3)_2][Ni(mnt)_2]$ [mnt^{2-} = maleonitriledithiolate; $[RBzPyN(CH_3)_2]^+$ = 1-(4′-*R*-benzyl)-4-dimethylaminopyridinium; *R* = CN(**1**), F(**2**)], with unusual magnetic properties have been prepared and characterized. Both **1** and **2** form a 3D network structure in which the $[Ni(mnt)_2]^-$ anions form a 1D magnetic chain for **1** and a stepwise stack for **2** *via* weak π…π stacking interactions, C…C or C…N short interactions between the neighboring anions. Magnetic susceptibility measurements in the temperature range 1.8–300 K indicated that **1** and **2** show unusual spin gap transition around 30 K and 110 K, respectively. The transition for **1** and **2** is the second-order phase transition as determined by the capacity measurement.

1. Introduction

The study of molecular magnets that possess spin bistability has attracted considerable attention due to their potential applications in molecular switch, data storage and displays [1–4]. Recently, one of the major research aims in this field is in spin transition molecular system containing $[M(mnt)_2]$ (*M* = Ni, Pd, or Pt ions, mnt^{2-} = maleonitriledithiolate) anion because such molecules possess a planar configuration with an extended electronic structure and the magnetic coupling is highly sensitive to the interaction contacts and the overlap patterns of $[M(mnt)_2]$ anions [5–9]. Substantial efforts have been devoted to finding more suitable counteractions to tune the crystal stacking structure of $[M(mnt)_2]^-$ ions with a view to obtaining ideal molecular magnets displaying a spin gap transition [10–12]. Herein, we selected organic cations, $[CNBzPyN(CH_3)_2]^+$ and $[FBzPyN(CH_3)_2]^+$ to tune the crystal stacking structure of $[Ni(mnt)_2]$ anion, and obtained two new molecular magnets, ($[CNBzPyN(CH_3)_2][Ni(mnt)_2]$)(**1**) and ($[FBzPyN(CH_3)_2][Ni(mnt)_2]$)(**2**), with an unusual spin gap transition around 30 and 110 K, respectively. Their molecular structures are schematically illustrated in Chart 1. It is very rare for $Ni(mnt)_2$ complexes that possess stepwise stack of the anions, and that exhibit novel spin gap features.

2. Experimental section

2.1. Materials and methods

All chemicals purchased were of reagent grade and used without further purification. The starting materials, disodium maleonitriledithiolate (Na_2mnt) and 1-(4′-*R*-benzyl)-4-dimethylaminopyridinium bromide $[RBzPyN(CH_3)_2]Br$ (*R* = CN(**1**), F(**2**)), were synthesized following the literature procedures [10]. Elemental analyses were run on a Model 240 Perkin-Elmer C H N instrument. IR spectra were recorded on IF66 V FT-IR (400–4000 cm^{-1} region) and NEXUS870 FT-IR (200–400 cm^{-1} region) spectrophotometers in KBr pellets. The heat capacities were performed using a Quantum Design PPMS in the temperature range 2–150 K. Magnetic susceptibility measurements were carried out in the temperature range 1.8–300 K using a Quantum Design MPMS XL superconducting quantum interference device (SQUID) magnetometer.

2.2. Syntheses of $[CNBzPyN(CH_3)_2][Ni(mnt)_2]$(**1**) and $[FBzPyN(CH_3)_2][Ni(mnt)_2]$(**2**)

$[CNBzPyN(CH_3)_2][Ni(mnt)_2]$(**1**) and $[FBzPyN(CH_3)_2][Ni(mnt)_2]$(**2**) were prepared according to a similar method described in literature [8]. Yield of **1**: ~88%. *Anal.* Calc. for $C_{23}H_{16}N_7NiS_4$: C, 47.85; H, 2.79; N, 16.98. Found: C, 47.79; H, 2.88; N, 16.79%. IR (cm^{-1}): 2210, 1444, 867, 398, 369 s. Yield of **2**: ~87%. *Anal.* Calc. for $C_{22}H_{16}FN_6NiS_4$: C,

* Corresponding author. Fax: +86 20 85282366.
E-mail address: ctgunicl@163.com (C.-l. Ni).

0022-4596/$ - see front matter © 2008 Elsevier Inc. All rights reserved.
doi:10.1016/j.jssc.2008.10.014

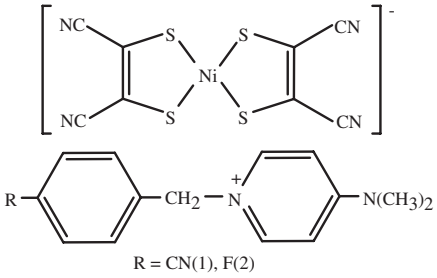

Chart 1. Molecular structure of **1** and **2**.

Table 1
Crystallographic data for **1** and **2** at 293 K

Compound	**1**	**2**
Molecular formula	$C_{23}H_{16}N_7NiS_4$	$C_{22}H_{16}FN_6NiS_4$
CCDC number	CCDC-297400	CCDC-676713
Molecular mass	577.38	570.36
Space group	*C*2/c	*P*−1
Crystal system	Monoclinic	Triclinic
a (Å)	32.772(7)	8.875(2)
b (Å)	7.251(2)	11.171(2)
c (Å)	21.444(4)	12.953(3)
α (deg)	90	100.06(1)
β (deg)	98.29(3)	92.56(1)
γ (deg)	90	99.86(1)
V/Å^3, *Z*	5043(2), 8	1242.1(4), 2
ρ (g cm^{-3})	1.521	1.525
μ (mm^{-1})	1.128	1.148
λ (Å)	0.71073	0.71073
F (000)	2360	582
Reflections collected	23189	6201
Independent reflections	4434	4288
$R_{(int.)}$	0.029	0.026
Goodness-of-fit on F^2	1.060	1.031
Final *R* indices [$I > 2\sigma(I)$]	$R_1 = 0.0340$	$R_1 = 0.0422$
	$wR_2 = 0.0862$	$wR_2 = 0.0902$
Final *R* indices (all data)	$R_1 = 0.0362$	$R_1 = 0.0639$
	$wR_2 = 0.0878$	$wR_2 = 0.0954$
Residual [eÅ^{-3}]	0.432 and −0.511	0.465 and −0.270

$R_1 = \Sigma(||F_o|-|F_c||)/\Sigma|F_o|$, $wR_2 = [\Sigma w(|F_o|^2-|F_c|^2)^2/\Sigma w(|F_o|^2)^2]^{1/2}$.

46.33; H, 2.83; N, 14.73. Found: C, 46.27; H, 2.92; N, 14.58%. IR (cm^{-1}): 2209, 1439, 868, 398, 373 s. Single crystals suitable for X-ray structure analyses were obtained by evaporating solution of **1** and **2** in mixed solution of MeCN and *i*-PrOH (1:2 v/v).

2.3. X-ray crystallography

Crystallographic data of **1** and **2** were collected using a Bruker Smart APEX CCD area detector with Mo-*K*α radiation ($\lambda = 0.71073$ Å) from a graphite monochromator. Structures were solved by direct methods and refined on F^2 by full-matrix least-squares, employing Bruker's SHELXTL [13]. All non-hydrogen atoms were refined with anisotropic thermal parameters. Hydrogen atoms were placed in calculated positions (C–H = 0.93 Å for benzene or pyridine rings, 0.96 Å for methyl groups, and 0.97 Å for methylene) and refined riding on their respective parent atoms with $U(H) = 1.2U$eq. Crystallographic details of **1** and **2** are listed in Table 1.

3. Results and discussion

3.1. Descriptions of structures

An asymmetric unit in a cell of **1** comprises an ion pair of $[Ni(mnt)_2]^-$ and $[CNBzPyN(CH_3)_2]^+$, as shown in Fig. 1a. The Ni ion in the $[Ni(mnt)_2]^-$ anion is coordinated by four sulfur atoms of two mnt^{2-} ligands in a square-planar coordination geometry. The bond distances and bond angles (Table 2) are in agreement with those of previously reported $[Ni(mnt)_2]^-$ compounds [6,8]. Four CN groups deviate slightly from the NiS_4 plane with the deviations −0.052 Å for C(1), −0.084 Å for N(1), 0.127 Å for C(4), 0.163 Å for N(2), −0.077 Å for C(5), −0.076 Å for N(3), 0.139 Å for C(8), and 0.243 Å for N(4). The dihedral angles in the $[CNBzPyN(CH_3)_2]^+$ between the benzene and pyridine rings to the reference plane, C(14)–C(15)–N(5), are 93.9° and 85.5°, respectively. As shown in Fig. 1b, the $[Ni(mnt)_2]^-$ and $[CNBzPyN(CH_3)_2]^+$ ions form a 3D network structure in which the Ni(III) ions form a 1D zigzag chain (Fig. 2a). Within an anionic chain, two overlap fashions between neighboring anions were depicted in Fig. 2b. The anions containing Ni(1) and Ni(1A)(symmetric code: A = −*x*, −*y*+2, −*z*) involves a $\pi\ldots\pi$ stacking interaction with the distance between C(2A) atom and the centroid of the molecular plane defined by S(1), S(2), C(2), C(3) and Ni(1) atoms is 3.522 Å, and the C…C short interaction is observed between the anions containing Ni(1) and Ni(1B) (symmetric code: B = −*x*, −*y*+1, −*z*) with the C(1)…C(2B) distance of 3.434 Å (Fig. 2a). The $\pi\ldots\pi$ stacking interactions, six weak C–H…N hydrogen bonds (Table 3) between neighboring anions and cations, and $\pi\ldots\pi$ interactions between the CN group and benzene ring (Fig. 2c) of cations further generate a 3D network structure.

The coordination geometry for the anion and the cation of **2**, which crystallizes in triclinic system with space group *P*−1, are essentially identical to those described above for **1**. The dihedral angles in the $[FBzPyN(CH_3)_2]^+$ between the benzene and pyridine rings to the reference plane, C(14)–C(15)–N(5), are 92.2° and 91.6°, respectively. Although **2** shows 3D network structure, the anions form stepwise stack (Fig. 3a) through $\pi\ldots\pi$ stacking interactions (the distance between atom Ni(1A) and the centroid of the molecular plane defined by S(3), S(4), C(6), C(7) and Ni(1) atoms is 3.653 Å, symmetric code: A = −*x*+1, −*y*+1, −*z*) and C…N short interactions (the C(1B)…N(2) and C(4)…N(1B) contacts is 3.359 and 3.405 Å, respectively, symmetric code: B = −*x*+1, −*y*+1, −*z*+1) between the neighboring anions (Fig. 3b). This stacking pattern is very rare for $Ni(mnt)_2$ complexes, and significantly different from that in **1.** The C–H…N hydrogen bonds between the anions and cations in **2** are listed in Table 3.

By comparing the structures of **1** and **2**, we conclude that the stacking and overlapping modes of the $[Ni(mnt)_2]^-$ anions are different when we have changed the *p*-substituted group in the benzene of benzyl group, and the *p*-substituted F and CN groups in the benzene favor a spin gap. In addition, some intermolecular contacts such as $\pi\ldots\pi$, C…N, C…C, and C–H…N weak interactions in **1** and **2** play important roles in the molecular stacking and magnetic coupling of **1** and **2**.

3.2. Infrared spectra

The ν(C≡N), ν(C=C), ν(C–S) and ν(Ni–S) bands of mnt^{2-} lie at 2230 and 2190, 1480, 865, 368 and 355 cm^{-1} for the starting $[Ni(mnt)_2]^{2-}$ salt of **1**, and 2213 and 2195, 1485, 862, 376 and 354 cm^{-1} for the starting $[Ni(mnt)_2]^{2-}$ salt of **2**. When the Ni(III) salts are formed, these bonds are at 2210, 1444, 867, 398 and 369 cm^{-1} for **1**, and 2209, 1439, 868, 398 and 373 cm^{-1} for **2**. These changes are similar to those of reported $[Ni(mnt)_2]$ salts [14].

3.3. Magnetic properties and heat capacity

The temperature dependences of the magnetic susceptibility for **1** and **2** in temperature range 1.8–300 K are shown in Fig. 4a

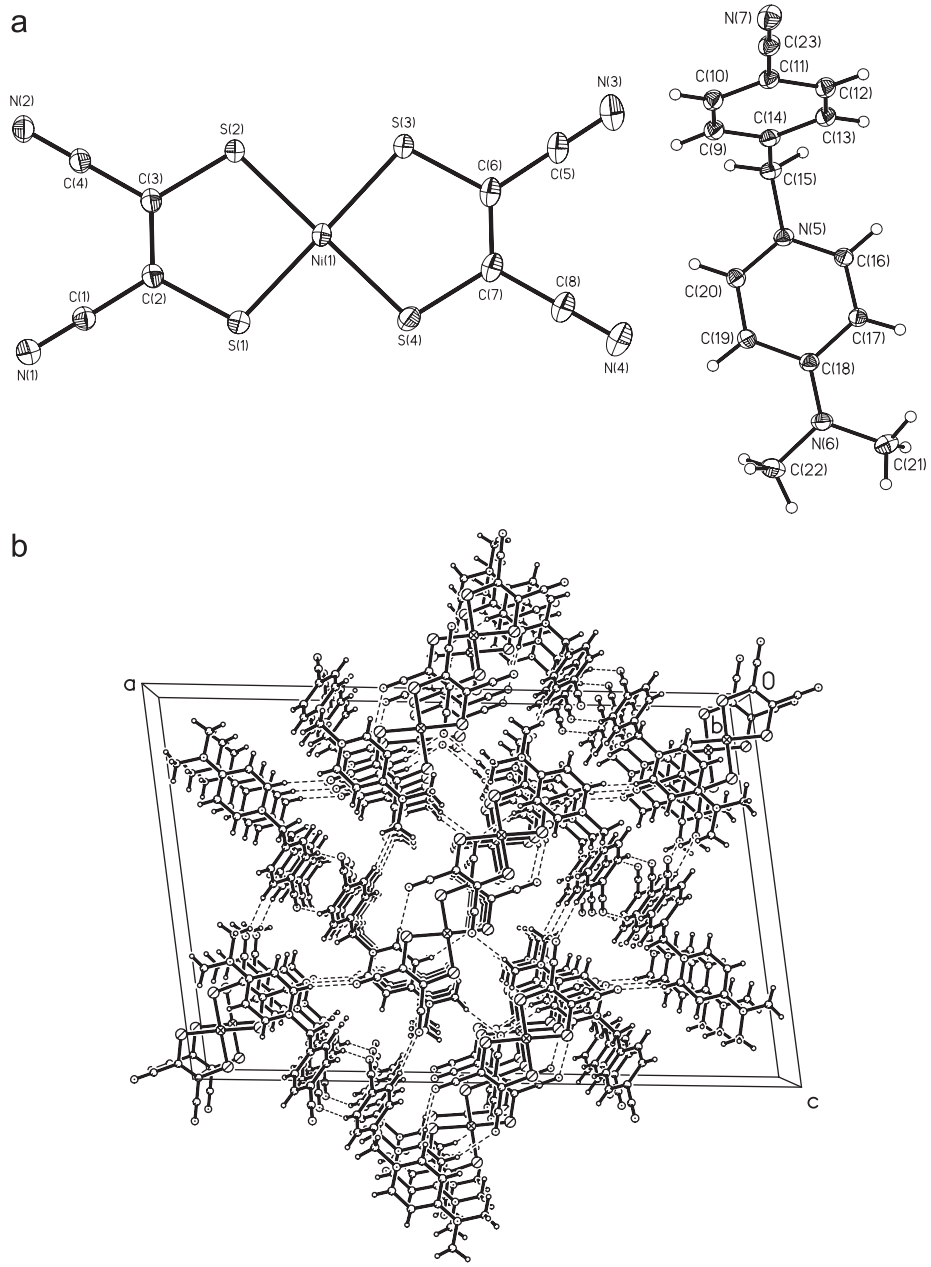

Fig. 1. (a) ORTEP plot (30% probability ellipsoids) showing the molecule structure of **1**. (b) The packing diagram of a unit cell for **1** as viewed along *b*-axis.

Table 2
Selected bond parameters and intermolecular contacts for **1** and **2**

Compound	**1**	**2**
Bond distances (Å)		
Ni(1)–S(1)	2.149(1)	2.139(1)
Ni(1)–S(2)	2.150(1)	2.147(1)
Ni(1)–S(3)	2.145(1)	2.138(1)
Ni(1)–S(4)	2.150(1)	2.141(1)
S(1)–C(2)	1.724(3)	1.709(3)
S(2)–C(3)	1.717(3)	1.720(3)
S(3)–C(6)	1.726(3)	1.707(3)
S(4)–C(7)	1.719(3)	1.704(3)
Bond angles (°)		
S(1)–Ni(1)–S(2)	92.79(4)	92.37(4)
S(1)–Ni(1)–S(4)	87.92(4)	87.50(4)
S(2)–Ni(1)–S(3)	87.02(4)	87.76(4)
S(3)–Ni(1)–S(4)	92.85(4)	92.35(4)

and b. The overall magnetic behaviors of **1** and **2** correspond to a paramagnetic system with an antiferromagnetic coupling interaction. As for **1**, upon cooling, firstly the χ_m values gradually increase to a maximum at 30 K, and below the temperature the χ_m values decrease abruptly to a minimum around 12 K, and finally increases again upon further cooling to 1.8 K. It is worthy to note that the χ_m values decrease exponentially around 30 K indicating that **1** undergoes a spin gap transition [15,16]. The transition temperature is evaluated as the temperature at the maximum of the $d(\chi_m T)/dT$ derivative, that is, ~30 K (inset of Fig. 4b).

Within the $[Ni(mnt)_2]^-$ anions chain of **1** (Fig. 2a), these NiS_4 planes are parallel, and the Ni(1)…Ni(1A) and Ni(1)…Ni(1B) distances are 6.151 and 7.826 Å, respectively. The distances between these NiS_4 planes are 3.491 Å for the anions containing Ni(1) and Ni(1A) atoms, and 3.456 Å for the anions containing Ni(1) and Ni(1B) atoms. From the structure analysis for **1** point of view, the degree of overlapping between the anions containing

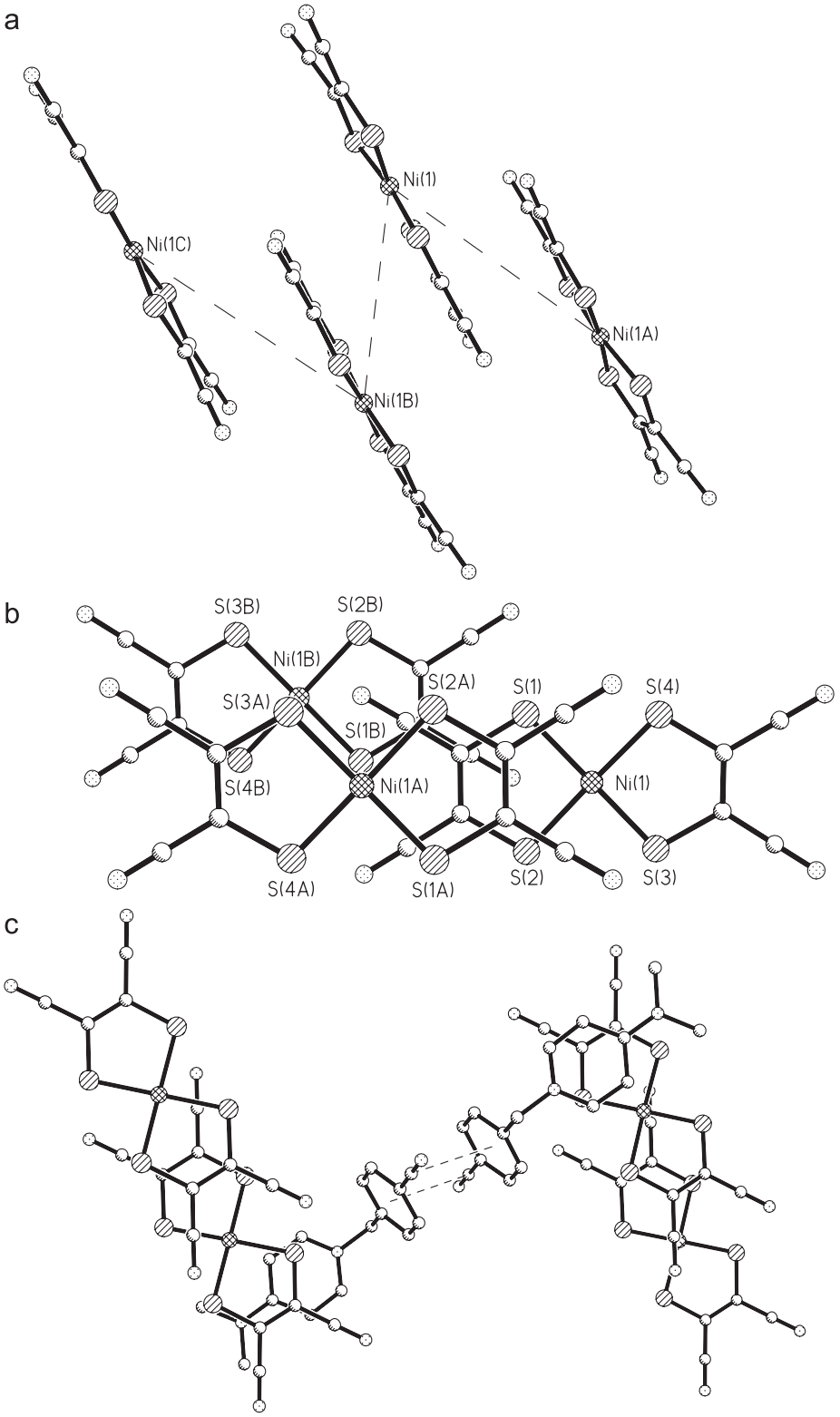

Fig. 2. Overlap patterns in 1D magnetic chain of $[Ni(mnt)_2]^-$ anions in **1**: (a) side and (b) top views. (c) The $\pi\ldots\pi$ stacking interactions in **1**.

Ni(1) and Ni(1A) atoms is larger than that of the anions containing Ni(1) and Ni(1B) atoms, therefore, the magnetic interaction between the anions containing Ni(1) and Ni(1A) atoms is larger than that of the anions containing Ni(1) and Ni(1B) in nickel(III) ions chain (Fig. 2a), therefore the magnetic susceptibility data of **1** in the high-temperature phase (30–300 K) can be modeled using simple dinuclear model approximation (the Hamiltonian being $H = -2JS_AS_B$) (Eq. (1)) [17]:

$$\chi_m = (2N\beta^2g^2/kT)(1-\rho)(3+\exp(-2J/kT)) + (N\beta^2g^2/2kT)\rho \quad (1)$$

where N, g, k, β and ρ have their usual meanings, and J is the exchange coupling parameter describing the magnetic interaction

between any two neighboring $S = \frac{1}{2}$ spins. Fitting the temperature dependence of magnetic susceptibility to Eq. (1) gives the reasonable parameters $g = 2.01$, $J = -44.6\,cm^{-1}$, $\rho = 0.146$ and $R = 2.3 \times 10^{-5}$ (R defined as $\Sigma(\chi_m{}^{calcd} - \chi_m{}^{obsd})^2/(\chi_m{}^{obsd})^2$). The magnetic susceptibilities in the low temperature may be estimated by the formula (Eq. (2)) [18]

$$\chi_m = \alpha \exp(-\Delta/kT)T + C/T + \chi_0 \quad (2)$$

where α is a constant value corresponding to the dispersion of excitation energy, Δ is the magnitude of the spin gap, χ_0 contributes from the core diamagnetism and the possible Van Vleck paramagnetism, and the other symbols have their usual meanings. The best fitting curve is shown in Fig. 4a, and the corresponding parameters are given as follows: $\alpha = 0.79$, $\Delta/k = 80.1\,K$, $C = 1.4 \times 10^{-3}\,emu\,K\,mol^{-1}$, $\chi_0 = 4.0 \times 10^{-4}\,emu\,mol^{-1}$, and $R = 2.2 \times 10^{-4}$.

As for **2**, upon cooling, firstly the χ_m values gradually increase to a maximum of 160 K, and below the temperature the χ_m values decrease abruptly to a minimum around 19.5 K, and finally increases again upon further cooling to 1.8 K. The transition temperature is evaluated as the temperature at the maximum of

Table 3
Weak hydrogen bonds for **1** and **2** (Å and deg)

D-H…A	d(D-H)	d(H…A)	d(D…A)	< (DHA)
Compound **1**				
C(10)–H(10)…N(7)#1	0.93	2.58	3.464(4)	158.0
C(12)–H(12)…N(3)#2	0.93	2.48	3.368(4)	159.0
C(16)–H(16)…N(2)#3	0.93	2.45	3.379(4)	178.0
C(17)–H(17)…N(1)#3	0.93	2.47	3.360(4)	161.0
C(20)–H(20)…N(4)#4	0.93	2.42	3.312(4)	160.0
C(21)–H(21B)…N(1)#5	0.96	2.62	3.314(4)	130.0
Compound **2**				
C(16)–H(16)…N(2)#6	0.93	2.45	3.261(5)	146.0
C(19)–H(19)…N(1)#7	0.93	2.53	3.425(5)	161.0
C(20)–H(20)…N(3)#8	0.93	2.58	3.458(5)	158.0

Symmetry transformations used to generate equivalent atoms: #1 = $-x+3/2$, $-y-1/2$, $-z+2$; #2 = $-x+1$, $y-1$, $-z+3/2$; #3 = $x+1$, y, $z+1$; #4 = $x+1/2$, $-y+3/2$, $z+1/2$; #5 = $-x+1$, y, $-z+1/2$; #6 = $x+1$, y, z; #7 = x, $y-1$, z; #8 = $-x+1$, $-y$, $-z$.

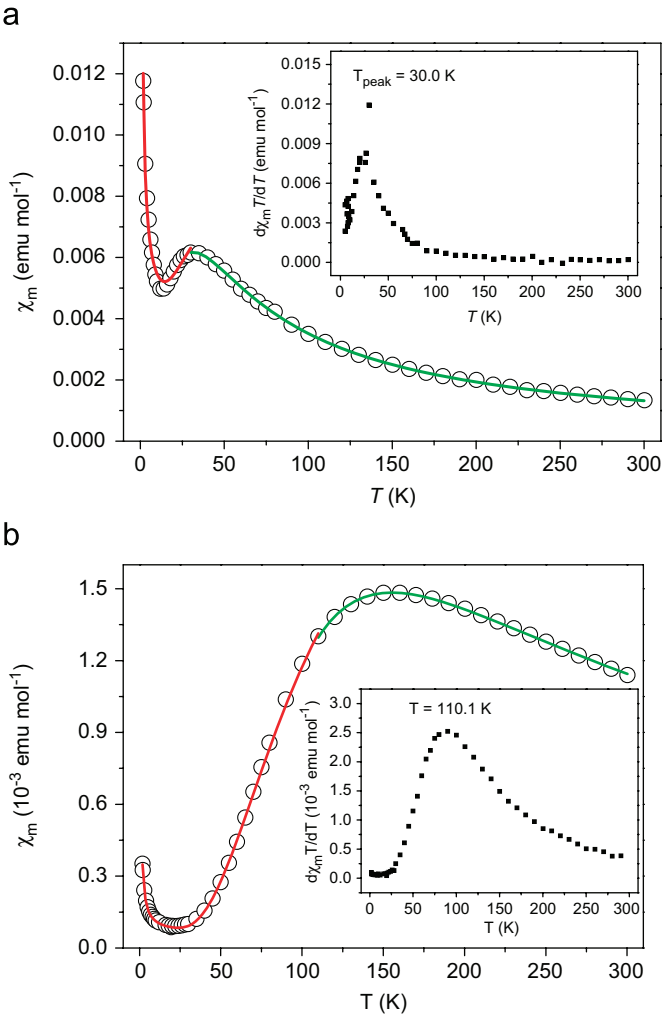

Fig. 4. Plots of χ_m vs T for **1**(a) and **2**(b) (inset: the plot $d(\chi_m T)/dT$ vs T). The solid lines (green: high-temperature phase; red: low-temperature phase) are reproduced from the theoretic calculations and detailed fitting procedure described in the text.

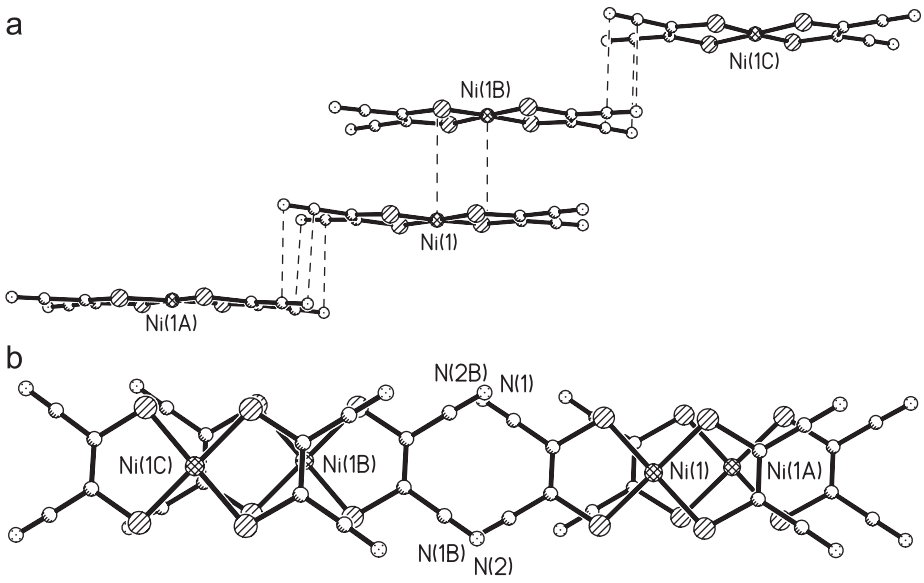

Fig. 3. (a) Stepwise stack of the $[Ni(mnt)_2]^-$ anions in **2**. (b) Top view of overlap patterns of $[Ni(mnt)_2]^-$ anions in **2**.

the d($\chi_m T$)/dT derivative, that is, ~110 K (inset of Fig. 4b). The experimental data of **2** may also be estimated by the formula (1) and (2), yielding the following parameters: $\alpha = 1.18$, $\Delta/k = 236.6$ K, $C = 5.2 \times 10^{-4}$ emu K mol^{-1}, $\chi_0 = 6.0 \times 10^{-5}$ emu mol^{-1}, and $R = 2.4 \times 10^{-4}$ within the range of 1.8–110 K, and $g = 2.02$, $J = -155.4$ cm^{-1}, $\rho = 9.6 \times 10^{-2}$, and $R = 8.4 \times 10^{-5}$ within the range of 110–300 K.

The results of the heat capacity measurement for **1** and **2** from 2 to 150 K show that no detectable peak in the corresponding temperature region was observed, indicating that the spin gap transition of **1** and **2** is the second-order phase transition [7].

The magnetic coupling between Ni(mnt)$_2^-$ anions is very sensitive to the overlap fashion of neighboring Ni(mnt)$_2^-$ anions and intermolecular contacts [4]. The magnetic exchange nature depends highly on the interplane distance (d) and the rotation angle (θ) [19]. Therefore, the magnetic behavior for **1** different from that of **2** may be understood. On lowering the temperature, the non-uniform compression of the magnetic chain and slippage of the Ni(mnt)$_2^-$ stack due to the anisotropic contraction of the crystal result in the magnetic exchange constant changing and trigger a spin gap transition [10].

4. Conclusion

In conclusion, the syntheses, crystal structures and magnetic properties of two new molecular magnets with [Ni(mnt)$_2$]$^-$ and substituted benzyl-4-dimethylaminopyridinium, have been investigated to achieve the novel spin gap system. Two molecular solids show a 3D network structure in which the [Ni(mnt)$_2$]$^-$ anions form a 1D magnetic chain for **1** and a stepwise stack for **2** *via* weak $\pi \ldots \pi$ stacking interactions, C…C or C…N short interactions between the neighboring anions. A novel spin gap transition around 30 K for **1** and 110 K for **2** are found. Antiferromagnetic interaction in the high-temperature phase (HT) and spin gap in the low-temperature phase (LT) are finely analyzed. The transition for **1** and **2** is the second-order phase transition as determined by the capacity measurement.

5. Supplementary materials

The detail crystallographic data of **1** and **2** have been deposited at the Cambridge Crystallographic Data Center as supplementary publication No. CCDC-297400 and No. CCDC-676713. Copies of the data may be obtained free of charge from The Director, CCDC, 12 Union Road, Cambridge, CB2 1EZ, UK (fax: +44 1223 336033; deposit@ccdc.cam.ac.uk or www: http://www.ccdc.cam.ac.uk).

Acknowledgments

The authors thank the Science and Technology Project (No. 20070B1000008) from Guangdong Science and Technology Department and the President's Science Foundation of South China Agricultural University (No. K05096) for financial support of this work.

References

[1] O. Kahn, C.J. Martinez, Science 297 (1998) 44.
[2] W. Fujita, K. Awaga, Science 286 (1999) 261.
[3] P. Gutlich, Y. Garcia, T. Woike, Coord. Chem. Rev. 219 (2001) 839.
[4] M.E. Itkis, X. Chi, A.W. Corde, R.C. Haddon, Science 296 (2002) 1443.
[5] J.L. Xie, X.M. Ren, Y. Song, W.W. Zhang, W.L. Liu, C. He, Q.J. Meng, Chem. Commun. (2002) 2346.
[6] M. Ren, Q.J. Meng, Y. Song, C.L. Lu, C.J. Hu, X.Y. Chen, Z.L. Xue, Inorg. Chem. 41 (2002) 5931.
[7] X.M. Ren, Q.J. Meng, Y. Song, C.S. Lu, C.J. Hu, Inorg. Chem. 41 (2002) 5686.
[8] C.L. Ni, D.B. Dang, Y. Song, S. Gao, Y.Z. Li, Z.P. Ni, Z.F. Tian, L.L. Wen, Q.J. Meng, Chem. Phys. Lett. 396 (2004) 353.
[9] A.T. Coomber, D. Beljonne, R.H. Friend, J.L. Brédas, A. Charlton, N. Robertson, A.E. Underhill, M. Kurmoo, P. Day, Nature 380 (1996) 144.
[10] X.M. Ren, S. Nishihara, T. Akutagawa, S. Noro, T. Nakamura, W. Fujita, K. Awaga, Chem. Phys. Lett. 418 (2006) 423.
[11] C.L. Ni, D.B. Dang, Y.Z. Li, S. Gao, Z.P. Ni, Z.F. Tian, Q.J. Meng, J. Solid State Chem. 178 (2005) 100.
[12] C.L. Ni, J.R. Zhou, Z.F. Tian, Z.P. Ni, Y.Z. Li, Q.J. Meng, Inorg. Chem. Commun. 10 (2007) 880.
[13] SHELXTL, Version 5.10. Structure Determination Software Programs, Bruker Analytical X-ray Systems, Inc., Madison, Wisconsin, USA, 2000.
[14] M.K. Johnson, Vibrational Spectra of Dithiolene Complexes in Dithiolene Chemistry, Progress in Inorganic Chemistry, Wiley, New York, 2004.
[15] Y. Fujii, T. Goto, W. Fujita, K. Awaga, Phys. B 329–333 (2003) 973.
[16] S. Nishihara, T. Akutagawa, T. Hasegawa, T. Nakamura, Chem. Comm. (2002) 408.
[17] Y. Song, D.R. Zhu, K.L. Zhang, Y. Xu, C.Y. Duan, X.Z. You, Polyhedron 19 (2000) 1461.
[18] L.C. Isett, D.M. Rosso, G.L. Bottger, Phys. Rev. B 22 (1980) 4739.
[19] Z.P. Ni, X.M. Ren, J. Ma, J.L. Xie, C.L. Ni, Z.D. Chen, Q.J. Meng, J. Am. Chem. Soc. 127 (2005) 14330.